ISSN 2095-6037
CN 11-2277/P

JMR Journal of Meteorological Research

Volume 39 Number 1 February 2025

气象学报(英文版)

Chinese Meteorological Society

Springer

JOURNAL OF METEOROLOGICAL RESEARCH

Vol. 39 No. 1 2025

CONTENTS

Chief Editor: Zhemin TAN Published Since 1987
Superintended by China Association for Science and Technology
Sponsored by Chinese Meteorological Society
Edited and Published by Editorial Office of *Journal of Meteorological Research*
Co-Published by Springer Nature
Produced by Beijing Renhe Information Technology Co. Ltd.
Printed by Beijing BOHS Color Printing Co. Ltd.
Domestically Distributed by China Science Publishing &Media Ltd.
Internationally Distributed by Springer Nature
Online Submission: http://jmr.cmsjournal.net
Domestic Register Number: CN 11-2277/P
Publication Date: 24 February 2025 (Vol. 39, No. 1)
Domestic Subscription Price: 450 RMB per year (bimonthly published, 6 issues)

The Relationship Scenarios between Boundary Layer Jet and Coastal Heavy Rainfall during the Pre-Summer Rainy Season of South China

Yu DU[1,2,3*] and Siyang YI[1]

1 *School of Atmospheric Sciences*, *Sun Yat-sen University*, *and Southern Marine Science and Engineering Guangdong Laboratory (Zhuhai)*, *Zhuhai* 519082

2 *Guangdong Province Key Laboratory for Climate Change and Natural Disaster Studies*, *Sun Yat-sen University*, *Zhuhai* 519082

3 *Key Laboratory of Tropical Atmosphere–Ocean System (Sun Yat-sen University)*, *Ministry of Education*, *Zhuhai* 519082

(Received 5 August 2024; in final form 22 October 2024)

ABSTRACT

In the pre-summer rainy season of South China, the occurrence of heavy rainfall (HR) near coastal regions, particularly in Yangjiang, is closely related to an upstream boundary layer jet (BLJ) over the northern South China Sea. The emergence of this BLJ is considered a crucial forecasting factor for coastal HR. However, the specific extent of the relationship between BLJ and HR remains unclear. In this study, utilizing 22-yr TRMM rainfall records and ERA5 data, we categorize four scenarios: HR with BLJ, HR without BLJ, no HR with BLJ, and no HR without BLJ in binary classification. It is found that during NoBLJ-HR events, even when the threshold of BLJ is not met, the low-level onshore wind fosters coastal convergence and facilitates moisture transport. Conversely, BLJ-NoHR events witness the BLJ penetrating further north, inducing inland convergence, accompanied by a dry environment. The attributes of the BLJ, encompassing its intensity, direction, and location, alongside linked moisture conditions, exhibit differences between HR and non-HR events. Based on a comprehensive indicator of correlation, we suggest a relatively optimal criterion to identify BLJ: maximum wind speed exceeding 8–10 m s^{-1}, wind direction falling within 180°–270°, the jet's core located south of 20°–21°N, and humidity near the core surpassing 0.016–0.017 kg kg^{-1}. This study provides a benchmark for predicting the occurrence of HR through presence of the BLJ.

Key words: boundary layer jet (BLJ), coastal heavy rainfall, binary classification

Citation: Du, Y. and S. Y. Yi, 2025: The relationship scenarios between boundary layer jet and coastal heavy rainfall during the pre-summer rainy season of South China. *J. Meteor. Res.*, **39**(1), 26–40, https://doi.org/10.1007/s13351-025-4138-x.

1. Introduction

Boundary layer jets (BLJs) are a frequent occurrence over the northern South China Sea, playing an essential role in extreme weather events across southern China (Du et al., 2015; Li and Du, 2021; Du et al., 2022; Huang et al., 2022). Characterized by maximum wind speeds in the lower atmosphere (below 1 km), BLJs are influenced by boundary layer processes, large-scale circulations, weather systems, and topography (Du and Rotunno, 2014; Du and Chen, 2019b).

Two branches of BLJ at 950 hPa are found on either side of Hainan Island, referred to as BLJ-WEST and BLJ-EAST, which often intensify together. These BLJs exhibit significant seasonal variations, peaking during the pre-summer season (April–June) (Kong et al., 2020; Dong et al., 2021; Du et al., 2022). Additionally, they display diurnal variations, with maximum intensity observed at night (Zhang et al., 2024). Unlike land-based BLJs, which can be explained by the nocturnal reduced friction causing inertial oscillation (Blackadar, 1957) and thermal forcing over sloping terrain (Holton, 1967, Du and Rotunno, 2014; Shapiro et al., 2016), marine BLJs are subject to a more intricate interplay of factors (Li and

Supported by the National Natural Science Foundation of China (42122033 and 42475002), Innovation Group Project of Southern Marine Science and Engineering Guangdong Laboratory (Zhuhai) (316323005), Guangdong Major Project of Basic and Applied Basic Research (2024A1515510005 and 2020B0301030004), and Key Innovation Team Fund of China Meteorological Administration (CMA2023ZD08).

*Corresponding author: duyu7@mail.sysu.edu.cn

Chen, 1998; Chakraborty et al., 2009; Jiang et al., 2010; Du et al., 2015). The BLJ-WEST emerges during the night due to intensified upstream wind over Indochina resulting from inertial oscillation, hydraulic jump effects in the lee of the Annamite Range, and the influence of Hainan Island's topography (Kong et al., 2020). On the other hand, the BLJ-EAST is primarily influenced by inertial oscillations resulting from large-scale sea breezes, further modulated by Hainan Island's thermal effects (Du and Chen 2019b; Dong et al., 2021).

BLJs significantly influence heavy rainfall (HR) along the South China coast by creating favorable dynamical and thermal conditions that regulate precipitation intensity and distribution near the coastline (Du and Chen 2018, 2019a; Li and Du, 2021; Huang et al., 2022; Shen and Du, 2023). They contribute to the initiation and growth of coastal convection through lifting mechanisms, including mesoscale convergence at the jet's terminus, frictional convergence along the coast, and topographic uplifting. These three mechanisms make roughly equal contributions to lifting (Du et al., 2020a; Du et al., 2020b). Ageostrophic winds within the BLJ manifest as confrontational and asymptotic convergence, associated with strong storms and expansive rain bands, respectively (Huang et al., 2022). While the BLJ-WEST enhances rainfall downstream in northern Guangxi, the BLJ-EAST intensifies rainfall in coastal regions of Guangdong (Yangjiang and Shanwei) (Du et al., 2022). The diurnal variation of BLJs also influences the diurnal pattern of coastal rainfall (Dong et al., 2021).

Given the impact of BLJs on coastal rainstorms, they could potentially serve as a primary indicator for predicting HR, particularly for the challenging prediction of warm-sector HR along the coast. Recently emerging artificial intelligence (AI)-based methods have been highly fruitful in weather prediction. For instance, Pangu-Weather from Huawei produces better deterministic forecasts based on reanalysis data than the world's best numerical weather prediction methods (Bi et al., 2023). Predictive datasets including geopotential, humidity, wind speed, and temperature are made available, while precipitation is not investigated in this model. This leads to an ideal method for predicting contemporary precipitation based on accurately predicted wind fields and other meteorological elements.

Therefore, clarifying the relationship between BLJ and HR is essential. Previous studies (Du and Chen 2019a, b; Li and Du 2021) have primarily documented how BLJs facilitate rainstorm occurrence and development, focusing on the co-occurrence scenario of BLJ and HR. However, in reality, their correspondence is not always perfect, leading to uncertainties in HR forecasting based on BLJ. Situations where BLJs are present without HR, and vice versa, have received limited attention. The varying identification criteria of BLJ can significantly affect the relationship between BLJ and HR occurrences. Addressing these disparities is crucial to enhancing our understanding of the detailed relationship between BLJ and HR, further promoting BLJ as an indicator for predicting HR occurrence. Therefore, this study aims to address two pivotal questions: (1) What underlines the non-correspondence between BLJ occurrences and coastal HR? (2) How can the correlation between BLJ and coastal HR be improved through refined BLJ identification criteria?

The primary objective of this paper is to explore the dynamic and thermodynamic factors contributing to coastal HR from a climatological perspective and employ this insight to improve their relevance. The paper is structured as follows: Section 2 describes the data, identification methods, and evaluation metrics. Section 3 compares the results of the four statistical scenarios. In Section 4, the statistical analysis highlights finer differences in BLJ distribution between HR and non-HR events. Section 5 presents sensitivity assessments probing the impact of BLJ criteria thresholds on relevance performance. Finally, Section 6 provides a discussion and summary.

2. Data and methodology

2.1 *Data used in this study*

The present study utilized Tropical Rainfall Measuring Mission (TRMM) observations to estimate rainfall, with a grid resolution of 0.25° × 0.25° (Huffman et al., 2007) and a temporal resolution of 3 h. TRMM, the pioneer satellite equipped with a rain-measuring radar, has been extensively applied in previous rainfall-related studies, and it demonstrates a strong ability to portray the characteristics of warm season precipitation in China (Shen et al., 2010; Chen et al., 2018; Li and Du, 2021).

To identify BLJ occurrences and analyze related environmental backgrounds, we applied the ECMWF fifth-generation atmospheric reanalysis (ERA5) dataset. ERA5 has a high spatial and temporal resolution, characterized by a horizontal grid spacing of 0.25° × 0.25° and a time interval of 1 h, allowing it to capture the intricate structure and evolution of BLJs (Du and Chen, 2019b; Kalverla et al., 2019; Chen et al., 2021; Li and Du, 2021; Du et al., 2022). Notably, while ERA5 also provides precipitation data that may align more closely with its dynamic and thermodynamic conditions compared to TRMM precipitation, it is important to note that ERA5 precipitation is primarily derived based on the ECMWF forecast model and can differ significantly from actual observations. This discrepancy is particularly evident in the coastal warm-sector heavy rainfall in South China, which is often misrepresented in ERA5. Therefore, we selected TRMM rainfall and ERA5 winds data to better capture real meteorological conditions, despite some inconsistencies between the wind field and precipitation data from the two different data sources.

The study's selected period covers the early summer rainy season (April to June) spanning from 1998 to 2019, marked by frequent heavy rainfall and BLJs along the southern coast of China (Du and Chen 2019b; Du et al., 2022). To maintain temporal consistency with the TRMM precipitation data, ERA5 data at 0000, 0300, 0600, 0900, 1200, 1500, 1800, and 2100 UTC each day are utilized in this study.

2.2 *Criteria for identifying BLJ*

Figure 1a presents the average 3-h cumulative precipitation distribution during the pre-summer rainy season, highlighting Yangjiang on the western coastline and Shanwei on the eastern coastline of Guangdong Province as two major hot spots of precipitation, consistent with previous studies (Zhang et al., 2022). Meanwhile, Fig. 1b shows strong low-level winds prevailing over the northern South China Sea, situated upstream of Yangjiang, indicating a high-frequency area of BLJs (Du et al., 2022). Given the spatial correspondence between rainfall in Yangjiang and its upstream BLJ, our focus gravitated toward the Yangjiang region and its coastal vicinity (21.375°–22.125°N, 111.875°–113.375°E) as the studied rainfall region for this investigation. The region characterized by strong southerly low-level winds upstream of the rainfall zone is regarded as the studied BLJ region (18°–21°N, 111.25°–113.5°E). Sensitivity tests were conducted on the selected region ranges, yielding statistically consistent outcomes across various range variations.

Based on long-term statistics of BLJs over the northern South China Sea (Du et al., 2022), a majority of BLJs exhibit southerly wind maxima at 950 hPa. Consequently, we adopted the BLJ identification criteria for this study in accordance with Li and Du (2021): (1) the maximum wind speed within the studied BLJ region at 950 hPa is ⩾ 10 m s^{-1}, and (2) the wind direction (calculated by averaging the u and v wind components within the BLJ region) must fall between 90° and 270°, ensuring the presence of southerly wind components. These BLJ criteria can be further fine-tuned based on factors such as strength and wind direction, which will be discussed later. We also evaluated the average wind speed within the studied BLJ region using a threshold of ⩾ 10 m s^{-1} as a criterion. The main statistical conclusions remained largely consistent with those presented in this study, indicating that our conclusions are not significantly influenced by the spatial resolution of the data.

2.3 *Criteria for identifying coastal heavy rainfall*

To ascertain the presence of heavy rainfall, we require that at least one grid point within the studied area (black box in Fig. 1a) records the 3-h accumulated precipitation of 20 mm or more. Consequently, all rainfall data are categorized into either HR events or non-HR events based

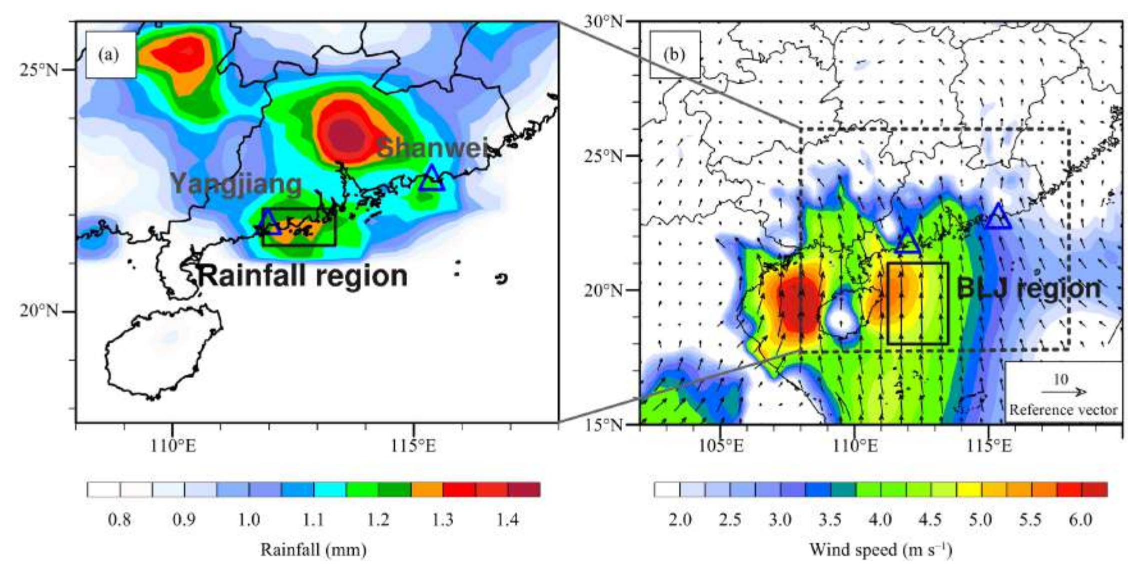

Fig. 1. Distributions of (a) 3-h cumulative precipitation (mm) and (b) horizontal wind speed (m s^{-1}) at 950 hPa in southern China during April–June of 1998–2019. The boxes with solid black borders in (a) and (b) correspond to the studied regions of rainfall and the BLJ, respectively. The blue triangles in (a) and (b) are indicative of locations of Yangjiang (west) and Shangwei (east) regions, respectively.

on this criterion. Many previous studies define HR by either 24-h accumulated precipitation exceeding 50 mm (Tao, 1980; Bao, 2007; Liu et al., 2020) or an hourly rainfall rate exceeding 15 mm h^{-1} (Chen et. al., 2007). Given that TRMM data has a 3-h time resolution, we ultimately selected a threshold of 20 mm to balance previous thresholds with statistical sample size requirements. Notably, a day is partitioned into 8 mutually independent events, which coordinate with the BLJ events. The temporal resolution of both BLJ occurrences and heavy rainfall is synchronized to enable correlation analysis.

Previous studies (Li and Du, 2021) documented that warm-sector heavy rainfall constitutes the dominant rainstorm type along the South China coast, as opposed to frontal heavy rainfall. Hence, this study refrains from distinguishing these two types. Furthermore, typhoon events are excluded from our dataset using typhoon path data sourced from the China Meteorological Network.

2.4 *Confusion matrix and evaluating indicators*

A confusion matrix is introduced for binary classification, serving to validate the prediction performance of the model (Townsend, 1971; Hastie et al., 2009; Sokolova and Lapalme, 2009; Powers, 2011; Murphy, 2012). It illustrates the relationship between predicted and actual labels by listing four basic metrics: true positive (TP), false positive (FP), false negative (FN), and true negative (TN), as shown in Table 1. A high proportion of TP and TN in all samples along the main diagonal of the confusion matrix signifies excellent prediction skills for the model.

Practical quantitative measurement indices based on the confusion matrix are defined to measure the performance of the model. Precision is defined as

$$\text{Precision} = \frac{\text{TP}}{\text{TP} + \text{FP}},$$

which indicates the ratio of true positives within the total predicted positives. The false alarm ratio equals 1 minus the Precision. Recall, on the other hand, is defined as

$$\text{Recall} = \frac{\text{TP}}{\text{TP} + \text{FN}},$$

reflecting the ratio of true positives in relation to the total actual positives. The miss ratio corresponds to 1 minus the Recall. It is important to note that Precision pertains to prediction results, while Recall relates to the original samples. Due to different measurement views, these two indexes may fluctuate in opposing directions in practical performance. Combining Precision and Recall, the F_1 score furnishes a comprehensive measure of the model's prediction effectiveness. The F_1 score is calculated by using the formula:

Table 1. Confusion matrix for binary classification

Confusion matrix		Predictive value	
		Positive	Negative
Actual value	Positive	TP	FN
	Negative	FP	TN

$$F_1 = \frac{1}{\frac{1}{2}\left(\frac{1}{\text{Precision}} + \frac{1}{\text{Recall}}\right)}.$$

This metric achieves a balance between correctly identifying positive cases and minimizing false positives. A higher F_1 score indicates a better balance between Precision and Recall, generally suggesting more effective classification performance. The F_1 score serves as a comprehensive metric that reflects both the false alarm ratio and the miss ratio in meteorological predictions.

Considering that the convergence at the exit of BLJ and the accompanying moisture transport by the BLJ over the northern South China Sea provide favorable conditions for coastal HR, further quantitative exploration of their correlation is a logical continuation. One of the simplest and most straightforward methods is utilizing the confusion matrix. Here, the presence or absence of the BLJ is treated as a positive or negative case for predictive value, while the presence or absence of HR is taken as positive or negative for actual value. Consequently, the evaluation indicators associated with the confusion matrix can be used to quantitatively characterize the extent of correlation between the two.

3. Differences among the four correlation regimes

Table 2 presents the confusion matrix for HR and BLJ based on the BLJ and HR criteria described in Section 2, employing a maximum wind speed threshold of 10 m s^{-1} to identify BLJ. Coastal HR occurs in only approximately 13% of BLJ events [960/(960 + 6357)], indicating a Precision of 13%. In other words, the absence of coastal HR characterizes the remaining 87% of BLJ events [6357/(960 + 6357)], resulting in a false alarm ratio of 87% based on BLJ occurrences. These results unexpectedly suggest that the presence of BLJs near the coast for extended periods does not invariably result in HR.

From an HR perspective, 68% of HR occurs in associ-

Table 2. Confusion matrix for HR and BLJ based on a maximum wind speed threshold set to 10 m s^{-1}

		BLJ	
		BLJ: Yes	BLJ: No
Heavy rainfall	HR: Yes	960	444
	HR: No	6357	7835

ation with BLJs, yielding a Recall of 68%. Only 32% of HR occurs without BLJs, indicating a miss ratio of 32%. These findings imply a strong association between coastal HR and BLJ, but certain HR instances can still materialize during non-BLJ events due to other influencing factors.

Most HR events are associated with BLJs, but only 13% of BLJ occurrences correspond with coastal HR, suggesting that while BLJs are somewhat necessary for heavy rainfall, they are not sufficient on their own. In other words, while the miss ratio remains relatively low, the false alarm ratio is high, possibly due to the relatively weak constraint of the jet criteria, resulting in a higher number of identified BLJs. This also highlights the imperative need to adjust the BLJ identification criteria to enhance correlation with HR.

Based on the results above, the correlation scenarios can be divided into four categories based on the terms of the confusion matrix (described in Section 2): BLJ-HR, NoBLJ-HR, BLJ-NoHR, and NoBLJ-NoHR.

Figure 2 displays composite rainfall distributions for the four correlation regimes. In the BLJ-HR regime (Fig. 2a), substantial 3-h cumulative precipitation exceeding 6 mm occurs along the coast of South China (Yangjiang–Pearl River Delta–Shanwei) spanning an extensive west–east range. In contrast, in the BLJ-NoHR regime (Fig. 2c), rainfall occurs inland in the northern Guangdong Province, northern Guangxi Province, and northern Fujian Province, but with less coastal precipitation. The NoBLJ-HR regime exhibits precipitation concentration

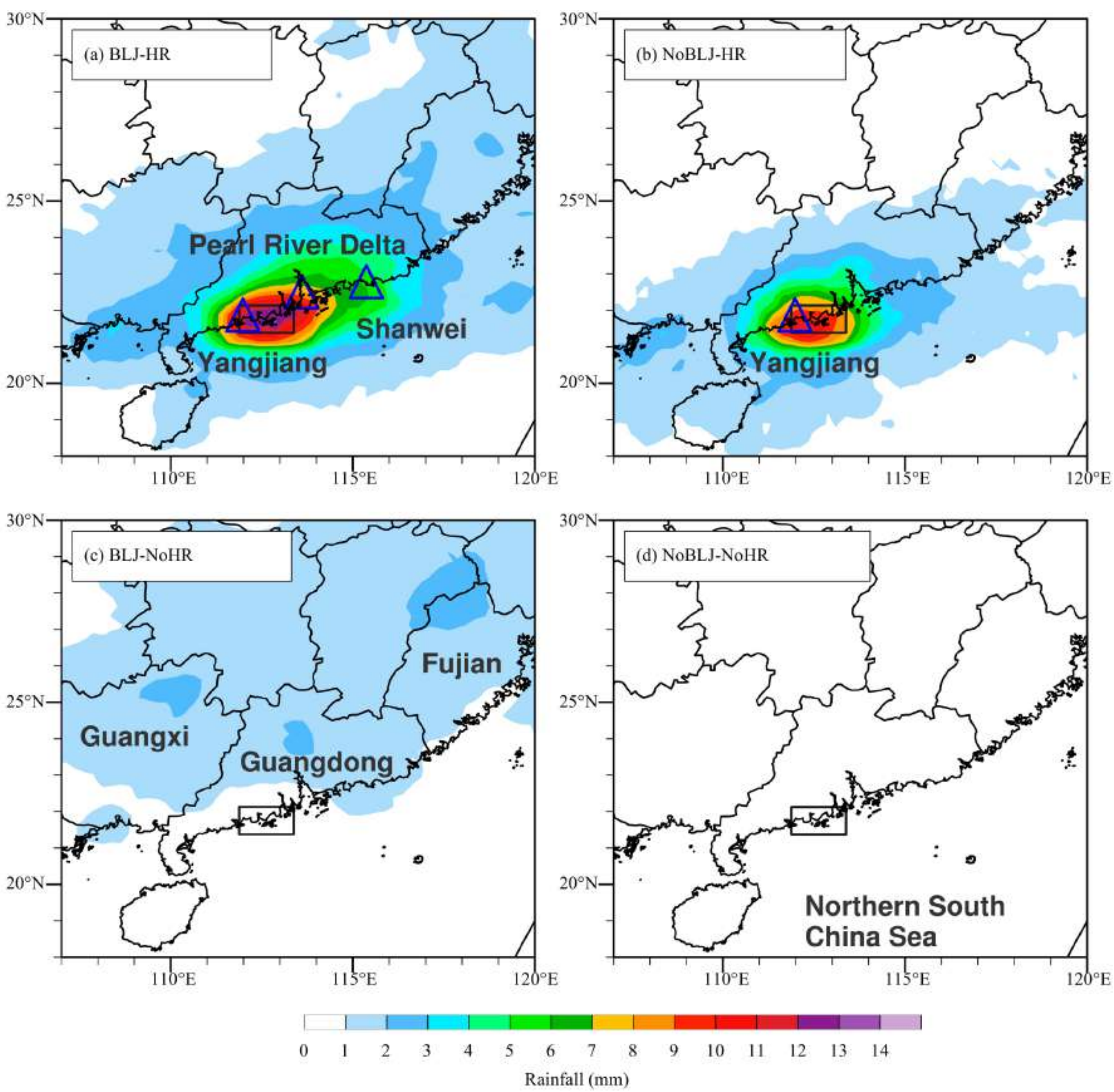

Fig. 2. Composite distributions of 3-h accumulated precipitation (mm) during the pre-summer rainy season (April–June) for four different groups: (a) BLJ-HR, (b) NoBLJ-HR, (c) BLJ-NoHR, and (d) NoBLJ-NoHR. The black boxe indicates the studied region of heavy rainfall. The blue triangles are indicative of locations of Yangjiang (west), Pearl River Delta (middle), and Shangwei (east) regions, respectively.

primarily along the western coast of Guangdong, specifically in Yangjiang, which is distinct from the BLJ-HR regime. Finally, the NoBLJ-NoHR regime shows minimal precipitation across South China and the South China Sea. Although coastal HR is absent in both scenarios, the NoBLJ-NoHR scenario aligns with expectations, while the BLJ-NoHR scenario warrants further investigation to understand the underlying mechanisms.

3.1 *Diurnal variations associated with the four regimes*

The diurnal variations are an important attribute of the BLJ and coastal precipitation, which are further explored among four different regimes in Fig. 3. For the BLJ-HR and NoBLJ-HR regimes (Fig. 3a), the occurrence frequencies peak in both the morning to midday hours around 0800–1400 LST (0000–0600 UTC; LST = UTC + 8 h), while fewer occur in the evening to dawn hours around 2000–0200 LST (1200–1800 UTC). In contrast, the weak peak frequency of the BLJ-NoHR regime is observed between 2300 and 0500 LST, consistent with the nocturnal intensification of the BLJ; while the NoBLJ-NoHR regime exhibits relatively consistent occurrence frequencies across all LSTs, lacking any significant diurnal variation.

Previous statistical studies have demonstrated that warm-sector HR near the coast frequently occurs in the morning (Li and Du, 2021), with which the frequency distribution pattern in Fig. 3a agrees. The diurnal variation of BLJ-HR more closely resembles that of the NoBLJ-HR regime with a peak in the morning but differs from the BLJ-NoHR regime with a peak at night. This suggests that the occurrence frequency within the BLJ-HR groups is more strongly driven by the diurnal variation of HR than by BLJ itself. Figure 3b compares the diurnal variation of composite wind speeds averaged over the BLJ region (Fig. 1b) among four regimes. Low-level wind speed is slightly higher in BLJ-HR than BLJ-NoHR across all LSTs, but both exhibit a similar trend over time (maximum wind speed occurs from midnight to early morning). Intriguingly, although the wind speed in the NoBLJ-HR group does not meet the jet's criteria, it still exhibits a slight diurnal variation trend similar to the first two groups. A counter example is the last group, the NoBLJ-NoHR regime is characterized by insignificant diurnal variations.

3.2 *Dynamics associated with the four regimes*

From a dynamic perspective, Fig. 4 provides a comparison of low-level winds across the four regimes. In the BLJ-HR regime, strong southwesterly winds with a core velocity of about 10 m s^{-1} occur over the northern South China Sea, adjacent to Hainan Island. This high-intensity southwesterly wind extends its impact to both the eastern (specifically Shanwei) and western coast (Yangjiang). The low-level wind distribution in BLJ-NoHR exhibits a similar structure to that in BLJ-HR, albeit with slightly weaker wind speeds. However, the winds in BLJ-NoHR shift predominantly to almost southerly instead of southwesterly and extend further north. The wind distribution in BLJ-NoHR more closely resembles the climatological average of BLJs (Du et al., 2022), primarily because BLJ-NoHR events are more frequent than BLJ-HR events. This also suggests that discerning the potential for heavy rainfall solely from the intensity

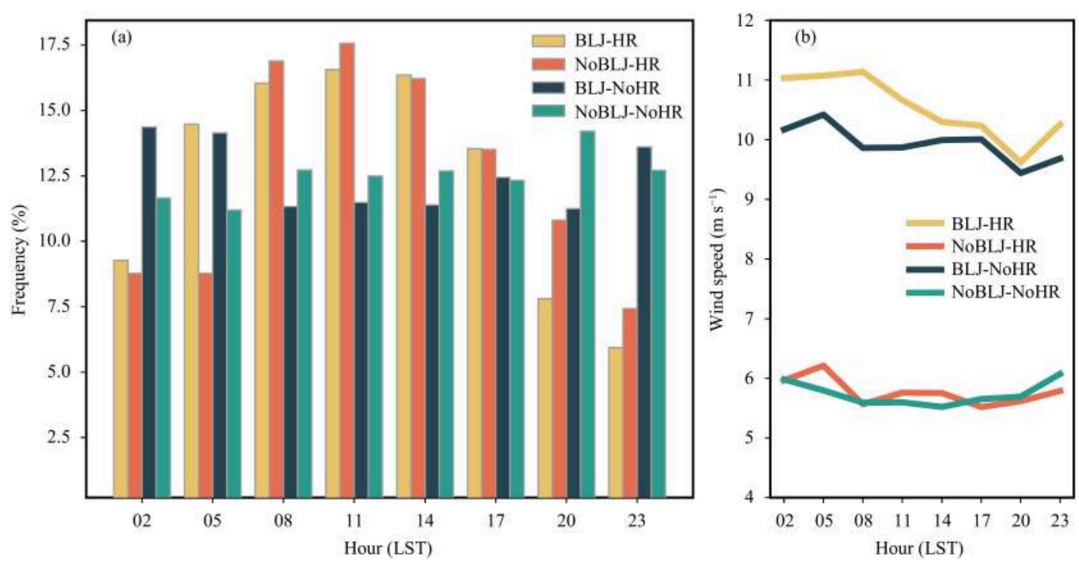

Fig. 3. Diurnal variations of the occurrence frequency (%) and wind speed (m s^{-1}) averaged over the BLJ region (Fig. 1b) for four different groups.

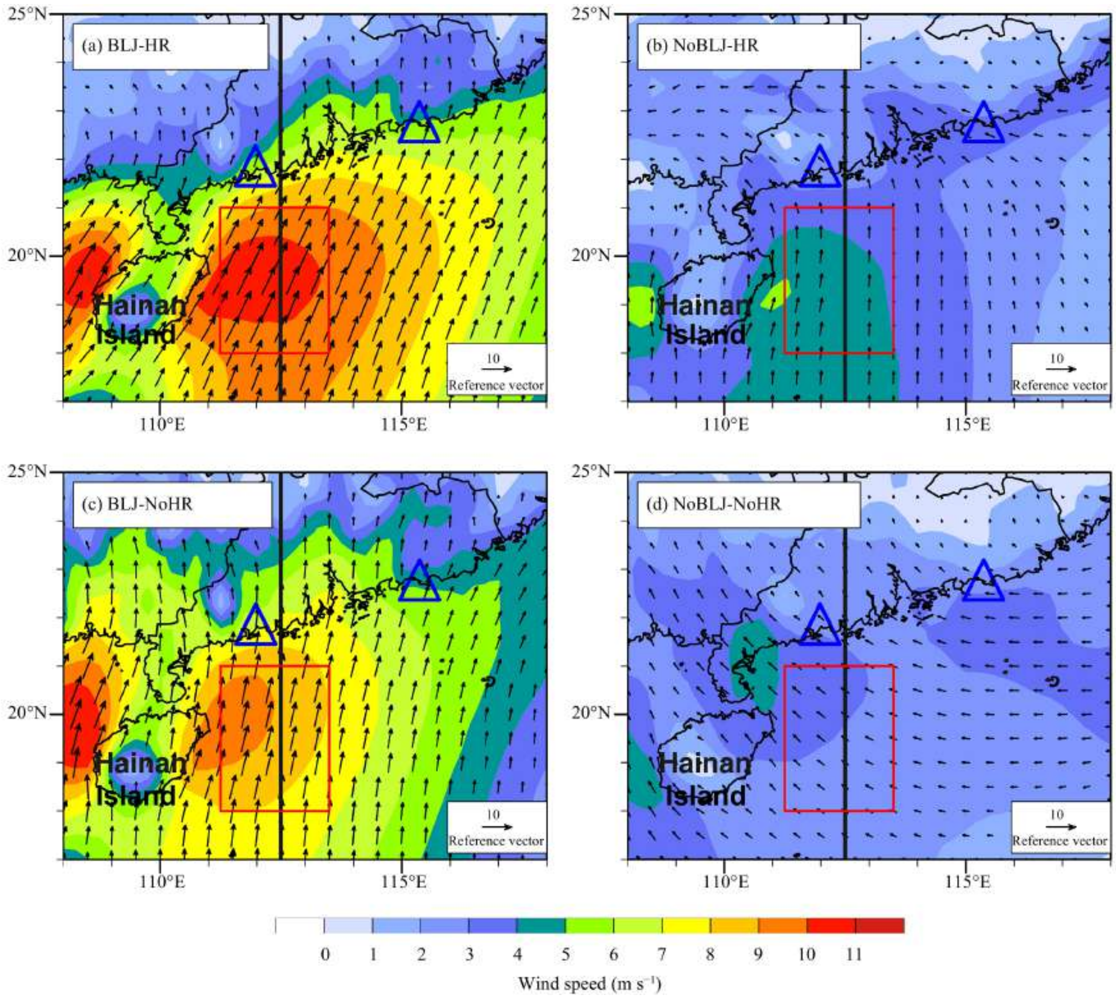

Fig. 4. As in Fig. 2, but with event-based average horizontal winds at 950 hPa (m s^{-1}). The red box indicates the area identified as the BLJ. The black lines are used in Fig. 5. The blue triangles are indicative of locations of Yangjiang (west) and Shanwei (east) regions, respectively.

of BLJs might not be sufficient. In the NoBLJ-HR regime, the low-level winds are almost perpendicular to the coast despite their relatively weak intensity. In contrast, the low-level winds in NoBLJ-NoHR are predominantly easterly and parallel to the coast. These results underline the scope for refining the BLJ criteria.

To illustrate the vertical structure of winds, Fig. 5 displays the latitude–height cross-section of divergence and meridional wind across different scenarios. In the BLJ-HR regime (Fig. 5a), the BLJ extends from the South China Sea to the coastal region, blocked by coastal topography, with intermittent intense convergence at approximately 22°N ($< -0.6 \times 10^{-1}$ s^{-1}). The NoBLJ-HR regime shows a similar distribution of *v*-winds and convergence as the BLJ-HR, albeit with notably weaker intensity and a narrower scope (Fig. 5b). Despite the reduced intensity, *v*-winds in the NoBLJ-HR regime still produce substantial coastal convergence, indicating that wind speed and coastal convergence are not simply positively correlated. However, in the BLJ-NoHR regime (Fig. 5c), the BLJ can extend farther north than in the BLJ-HR regime. With the jet core located near the coastal area (about 20°N), the jet has sufficient momentum to pass over the Yangjiang mountains range, prompting inland convergence. In the NoBLJ-NoHR regime, the intensity and extent of coastal convergence are significantly weaker compared to the other three regimes, suggesting that the dynamical conditions supporting precipitation are less favorable (Fig. 5d).

3.3 *Thermodynamics associated with the four regimes*

Beyond dynamical convergence facilitated by the BLJ, the occurrence of HR is also influenced by prevailing thermodynamic environmental conditions. Figure 6 compares the horizontal distributions of specific humidity at 950 hPa across the four forecast regimes. In the BLJ-HR regime (Fig. 6a), a south–north oriented high moisture tongue (> 0.017 kg kg^{-1}) emerges, originating from the middle of the South China Sea and extending to the

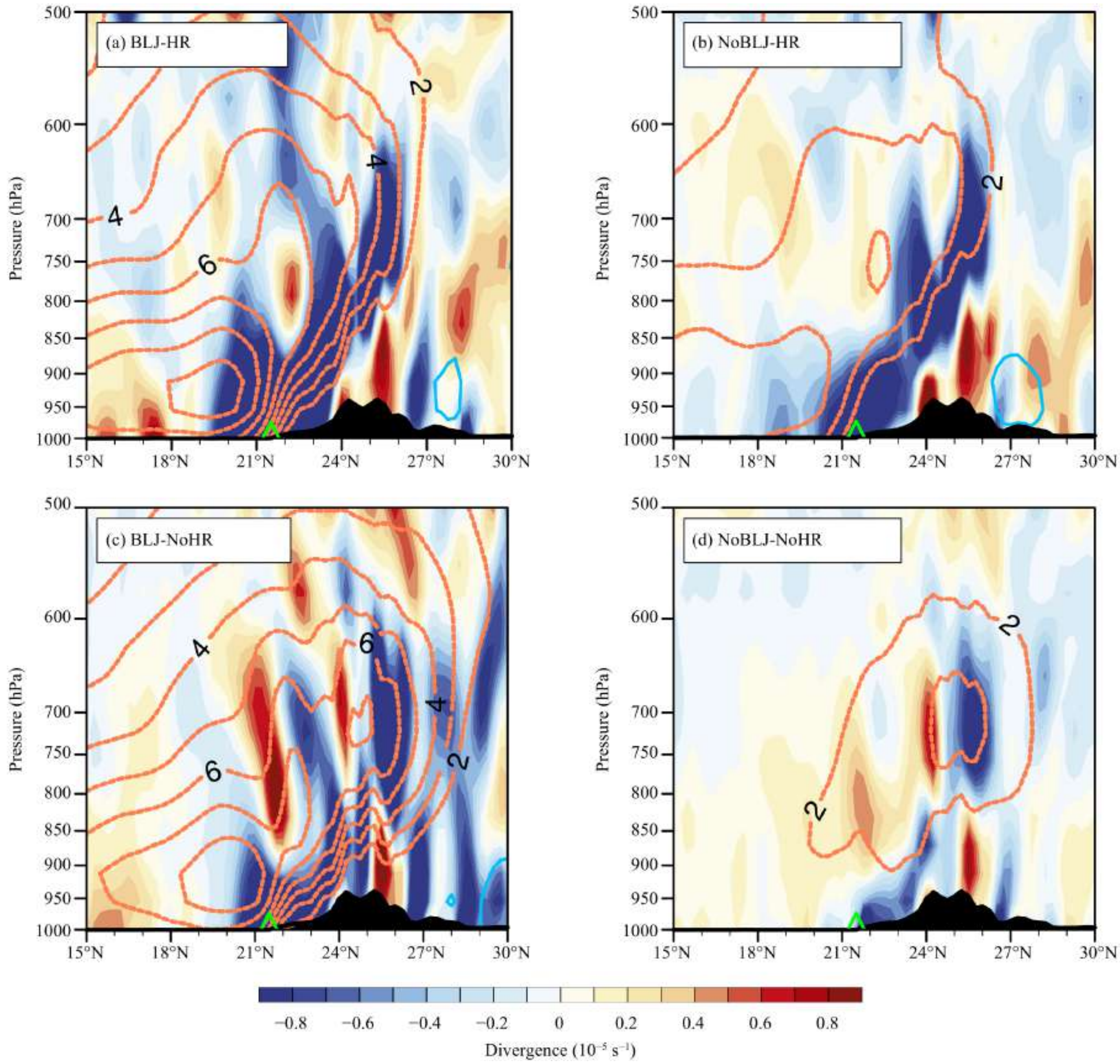

Fig. 5. Vertical cross-sections of divergence (shading, red for divergence and blue for convergence; 10^{-5} s^{-1}) and meridional wind speed (dotted lines; m s^{-1}) along 112.5°E (black line in Fig. 4) for four different groups: (a) BLJ-HR, (b) NoBLJ-HR, (c) BLJ-NoHR, and (d) NoBLJ-NoHR. The green triangle denotes the location of the coast, while the black shading represents the terrain.

coast. This abundance of water vapor transported by BLJs provides favorable conditions for HR. The NoBLJ-HR regime presents a similar high moisture zone, albeit with slightly weaker intensity and northward extension (Fig. 6b). Despite BLJ presence in the BLJ-NoHR regime, the moisture tongue is not as pronounced as in BLJ-HR (Fig. 6c), indicating inadequate moisture supply. The NoBLJ-NoHR regime (Fig. 6d) shows the driest conditions among the four regimes across both inland and coastal regions, with concentrated high moisture exclusively occurring offshore in the central South China Sea.

Figure 7 compares the vertical profiles of humidity and wind averaged over the BLJ region across the four regimes. Interestingly, the NoBLJ-HR regime exhibits lower near-surface humidity due to weaker winds below 925 hPa. Despite this, humidity above 925 hPa is the highest or very close to the highest among the four regimes. In contrast, the BLJ-NoHR regime presents a shallow humidity layer. Despite high humidity below 950 hPa due to strong moisture transport by BLJ, it rapidly decreases with altitude. The remaining two regimes exhibit a synchronous pattern of wind speed and humidity. In the BLJ-HR regime, the effective transport of higher wind speeds (> 7 m s^{-1}) at all low levels promotes increased humidity. In the NoBLJ-NoHR regime, both low wind speeds (< 4 m s^{-1}) in the middle and lower layers and the driest environment (< 0.012 kg kg^{-1}) contribute to humidity scarcity.

The BLJ is recognized as a high transport zone for both momentum and water vapor. In addition to disparities in wind speed, moisture variability due to BLJs significantly impacts HR. Consequently, it is reasonable and

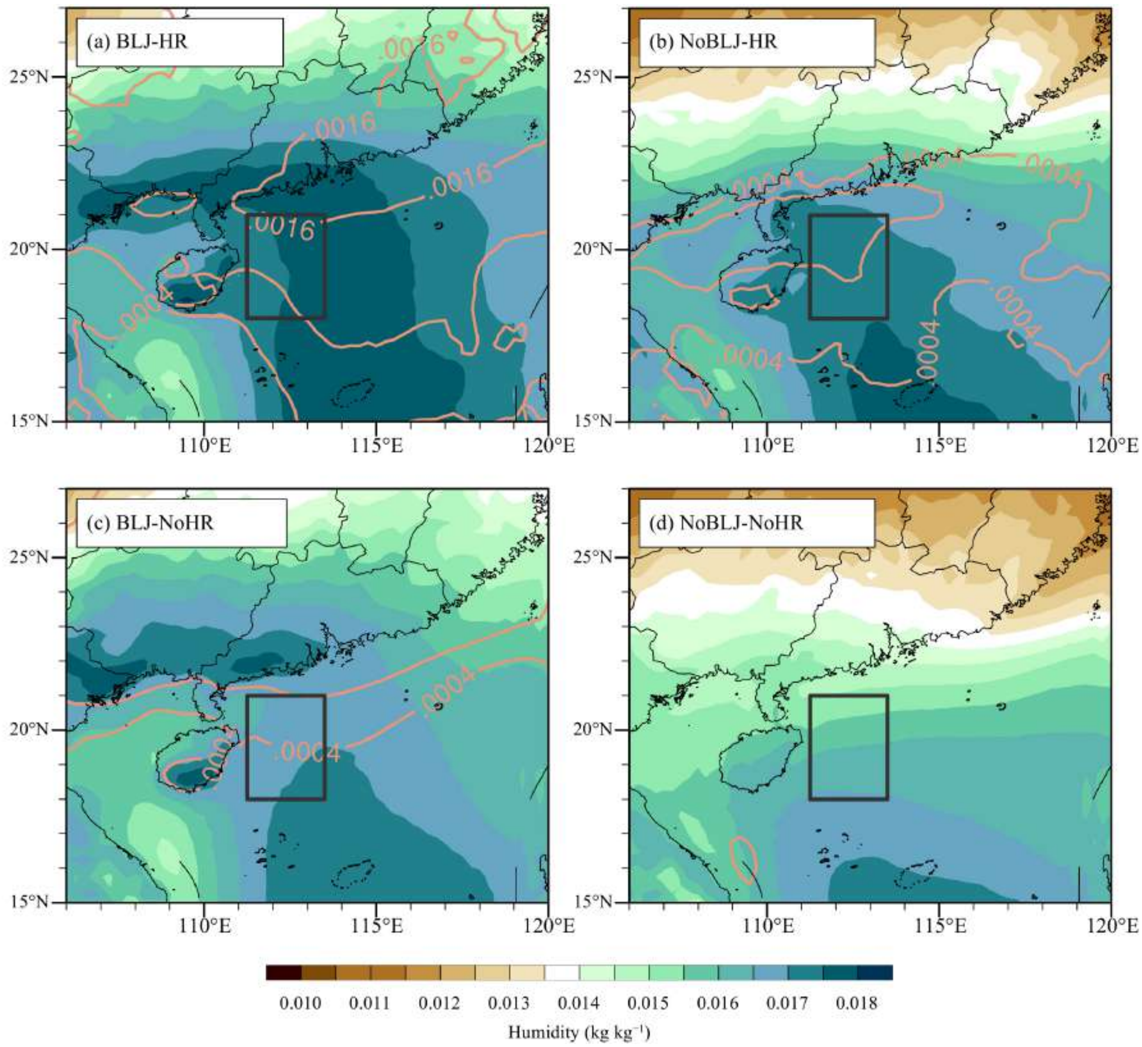

Fig. 6. As in Fig. 2, but with event-based average humidity at 950 hPa (kg kg^{-1}). The orange contours represent the differences in surface humidity between each group and the 22-yr climate average. The black box indicates the BLJ region.

necessary to consider both wind and humidity when establishing BLJ criteria, as further discussed in the subsequent sections. For instance, BLJs can be categorized as either "wet jets" or "dry jets."

4. Differences in BLJs between HR and non-HR events

To enhance our comprehension of BLJs' behavior and their relation to HR occurrences, we conducted a thorough comparison in the characteristics of BLJs between HR and non-HR events. Our focus is on their intensity, wind direction, location, and associated moisture, with the intention of capturing subtle differences for identifying BLJs more conducive to triggering HR conditions.

4.1 *Wind speed of the BLJ*

Figure 8a presents the frequency distribution of the maximum wind speeds of the BLJ core during HR and non-HR events. The occurrence frequency of HR-triggered BLJ increases within the range of 10–13 m s^{-1} of the jet core, and then decreases within the range of 13–18 m s^{-1}. The majority of the BLJs fall within the 10–15 m s^{-1} range, peaking at 12–13 m s^{-1}. In contrast, BLJs that do not trigger HR exhibit lower velocities, with the peak frequency at 10–11 m s^{-1}. These findings suggest a correlation between BLJ intensity and HR occurrences, with BLJs exhibiting moderate wind speeds being the most frequently associated with triggering heavy rainfall. Additionally, we calculated the proportion of BLJs during HR days relative to the total BLJs (green line in Fig. 8a). Notably, moderately intense BLJs are more likely to induce HR compared to weak or strong BLJs [except for BLJs that are particularly strong (> 19 m s^{-1}) but have small samples].

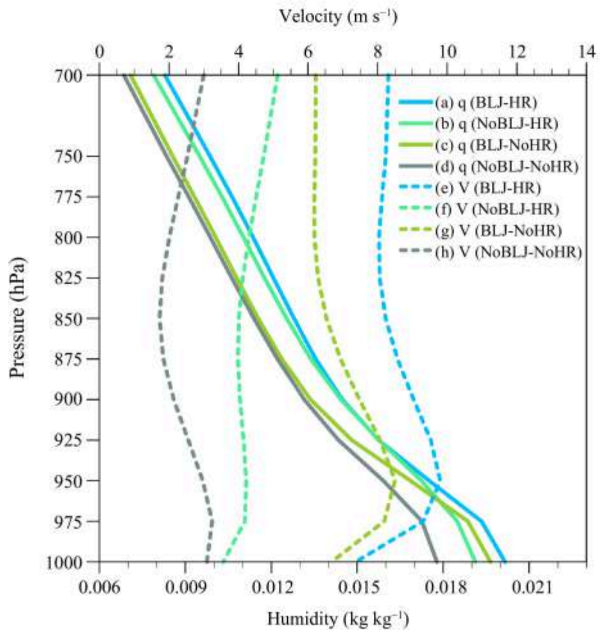

Fig. 7. Vertical profiles of horizontal wind speed (dashed lines; m s^{-1}) and humidity (solid lines; kg kg^{-1}) averaged over the BLJ region (Fig. 1b) for four different groups. The differences between the BLJ-HR and BLJ-NoHR, and those between NoBLJ-HR and NoBLJ-NoHR, are significant at the 95% confidence level by a two-tailed Welch's *t*-test.

4.2 *Wind direction of the BLJ*

During early summer in the northern South China Sea, the prevailing low-level winds are typically southwesterly at the time of BLJ occurrence (Fig. 8b), occasionally displaying an easterly component. BLJs during HR events predominantly fall within the wind direction range of 180°–220°, while on non-HR events, the pattern remains similar, albeit with a higher frequency of below 180° compared to HR events. Moreover, the proportion of BLJs causing HR within specific wind direction (the green curve in Fig. 8b) further indicates that BLJs within the 190°–240° wind direction range are more likely to be associated with HR.

BLJs within this wind direction range (190°–220°) are characterized by a stronger u-component than those associated with purely southerly winds. This phenomenon can be understood from the perspective of large-scale water vapor transport, where the southwesterly BLJ after the onset of monsoon circulation transports moisture from the Indian Ocean, thereby resulting in favorable moisture conditions for heavy rainfall.

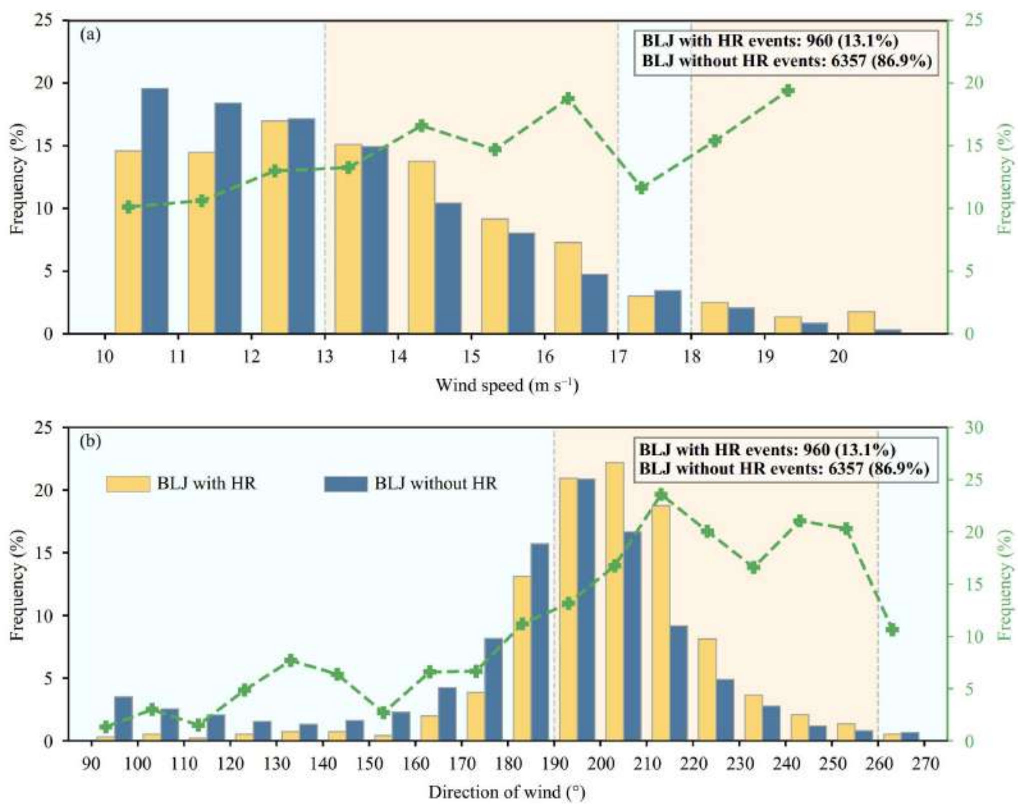

Fig. 8. Frequency distributions of key parameters related to the BLJ during HR events (yellow bars) and non-HR events (blue bars). The key parameters examined are (a) the maximum wind speed at the center of BLJs and (b) the mean wind direction of BLJs. The green lines indicate the proportion of BLJ occurrences during HR events relative to the total number of BLJs in that specific interval, representing the probability of the BLJ causing heavy rainfall within the corresponding parameter range. The differences between the means are significant at the 95% confidence level, as indicated by a two-tailed Welch's *t*-test.

4.3 *The location of the BLJ*

Previous studies have paid little attention to the spatial characteristics of BLJs and their correlation with HR. However, the location of the BLJ can affect the moisture convergence at its exit, consequently impacting the location and intensity of the precipitation. In this study, we define the core of BLJs as a representation of their morphological characteristics. The core is determined by weighting wind speed with grid latitude and longitude for grid points that meet two conditions: (1) wind speed satisfies the preset BLJ wind speed criteria (10 m s^{-1}) and (2) the wind exhibits southerly wind components in the region shown in Figs. 9a, b (15°–24°N, 110°–118°E). Figures 9a, b show that the BLJ core locations on HR and non-HR days are generally similar, with some exceptions where BLJ cores in non-HR events are concentrated on the northeast side of Hainan Island near the coast, and even on land. Notably, Fig. 9c clearly demonstrates the spatial differences in BLJ cores on HR and non-HR events, with mean latitudes and longitudes for HR day BLJ cores approximately 19.2°N and 113.2°E, and in non-HR events BLJ cores around 19.7°N and 112.8°E. Furthermore, Fig. 9d also shows that BLJ cores at lower latitudes, particularly within 18°–19°N, are more prone to causing coastal HR. Additionally, when the jet core is located at a distance from the coast, the BLJ convergence zone aligns precisely with the coast.

4.4 *Humidity associated with BLJ*

From the preceding analysis, it was determined that humidity within BLJs is higher in HR events compared

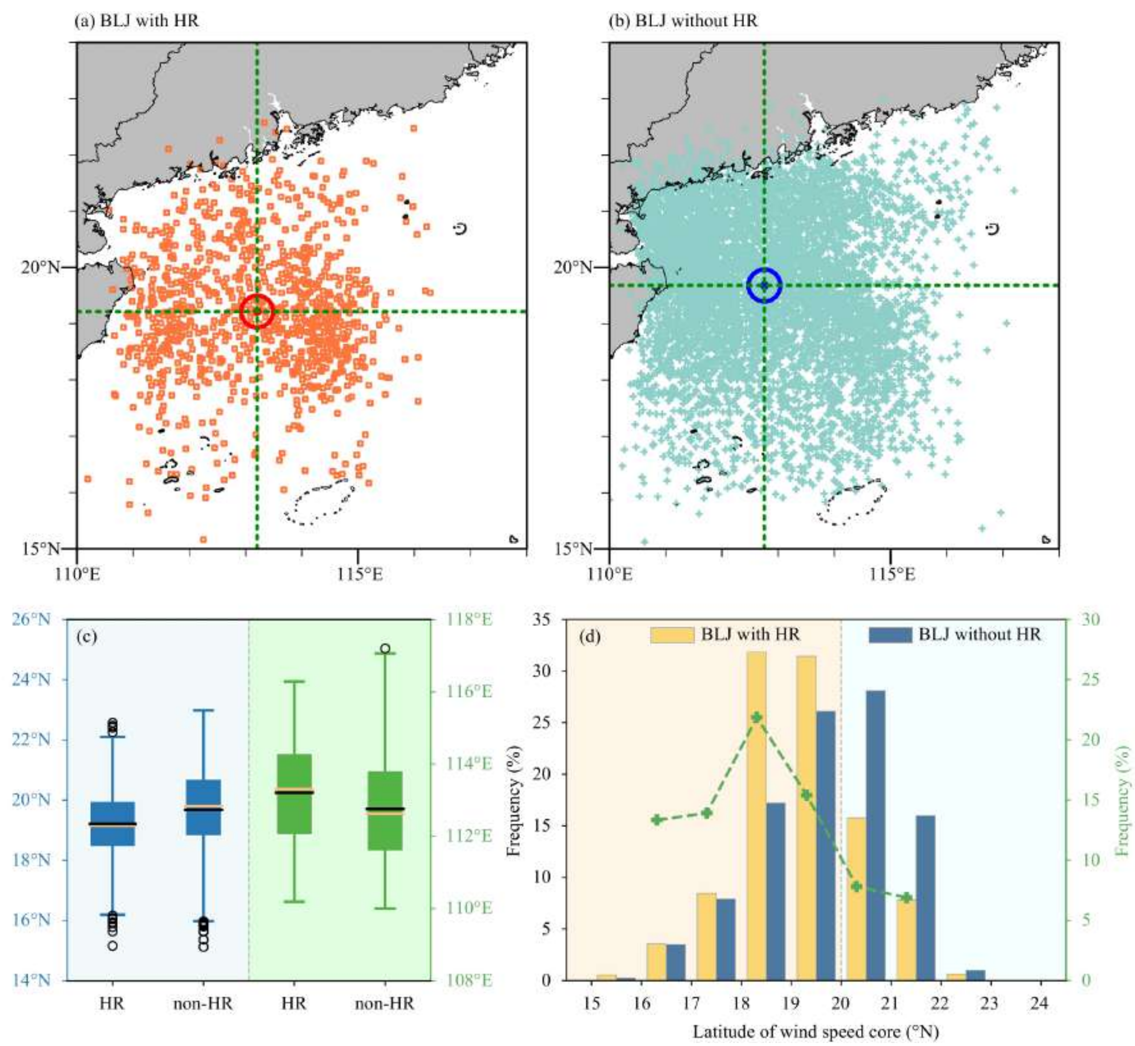

Fig. 9. Spatial distributions of the BLJ cores during (a) HR events and (b) non-HR events. The green dashed lines indicate the mean latitude and longitude of the BLJ cores. (c) The boxplot of latitudes and longitudes of the BLJ cores during HR events and non-HR events. The yellow (black) solid lines indicate the median (mean) values. The differences are significant at the 99% confidence level by two-tailed Welch's *t*-test. (d) The frequency distribution of the latitudes of the BLJ cores for HR events (yellow bars) and non-HR events (blue bars). The green dashed line indicates the proportion of BLJs occurring within HR events relative to the total number of BLJs in that specific interval.

to non-HR events. To further investigate this aspect, Fig. 10 compares the frequency distributions of mean humidity within the BLJ region during jets' occurrence between HR and non-HR events. The humidity within HR-triggering BLJs concentrates within a high humidity interval, peaking at 0.017–0.018 kg kg^{-1} (Fig. 10). On the other hand, more than 20% of BLJs on non-HR events exhibit low humidity (< 0.016 kg kg^{-1}), indicating insufficient moisture. Notably, when humidity exceeds 0.017 kg kg^{-1} (blue dashed line), The occurrence frequency of HR-associated BLJ in distribution exceeds those on non-HR events. The green line demonstrates a monotonic increase in probability with increasing humidity, indicating a stronger likelihood of HR initiation with higher moisture in BLJ.

5. Sensitivity of BLJ's criterion based on the relevance to HR

In Section 3, we presented qualitative analyses of the relationship between BLJ and HR, highlighting the influence of environmental conditions accompanying BLJ on precipitation, including the spatial distribution of wind and humidity. Section 4 provides a more intricate comparison of BLJ characteristics on HR and non-HR events, encompassing disparities in intensity, wind direction, location, and associated humidity. In this section, we conduct sensitivity assessments to refine the criteria for identifying BLJ as a singular consideration for inferring heavy rainfall occurrence. This analysis proceeds in two steps: defining BLJ using varying criteria, and assessing correlation performance using F_1 score as an indicator.

5.1 *Wind maximum speed thresholds*

Figure 11a illustrates the variability of the F_1 score with different wind speed thresholds for defining BLJ occurrence. The results show that the F_1 score reaches its peak at 12 m s^{-1}, with 11 and 10 m s^{-1} as the second-best options, indicating that moderate wind speeds are most conducive to predicting HR events. Wind speed thresholds below 10 m s^{-1} or above 15 m s^{-1} result in lower F_1 scores, suggesting inappropriate criteria. The optimal wind speed threshold might need adjustment based on specific conditions.

5.2 *Wind direction and latitude of jet core*

Figures 11b, c explore the impact of wind direction and latitude of the jet core on the F_1 score. The score improves significantly when wind direction thresholds are between 180° and 190°. The F_1 score peaks at 20°N for the upper limit of the jet core's latitude, when the wind speed thresholds are between 9 and 12 m s^{-1}. However, this optimal state is absent for higher wind speed thresholds (14 m s^{-1}). A lower wind speed threshold combined with limitations on the latitude of the jet core shows the most notable improvement. These results underscore the significant impact of jet location on overall relevance.

5.3 *Humidity thresholds*

Figure 11d evaluates the effect of humidity thresholds on the F_1 score. The most of the score peaks at a humidity of 0.017 kg kg^{-1}, indicating that higher moisture levels within the BLJ region are more likely to lead to HR. This supports the idea of categorizing BLJ as "wet jets" when humidity conditions are sufficiently high.

5.4 *Comprehensive Analysis*

Figure 12a further provides a comprehensive sensitivity analysis integrating wind speed, wind direction, latit-

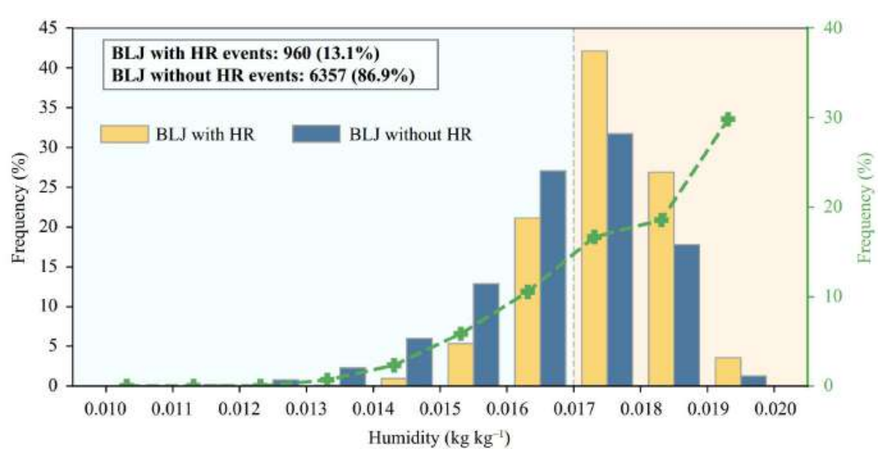

Fig. 10. As in Fig. 9d, but with the spatial average humidity of the BLJ. The differences between BLJ-HR and BLJ-NoHR are significant at the 95% confidence level by two-tailed Welch's *t*-test.

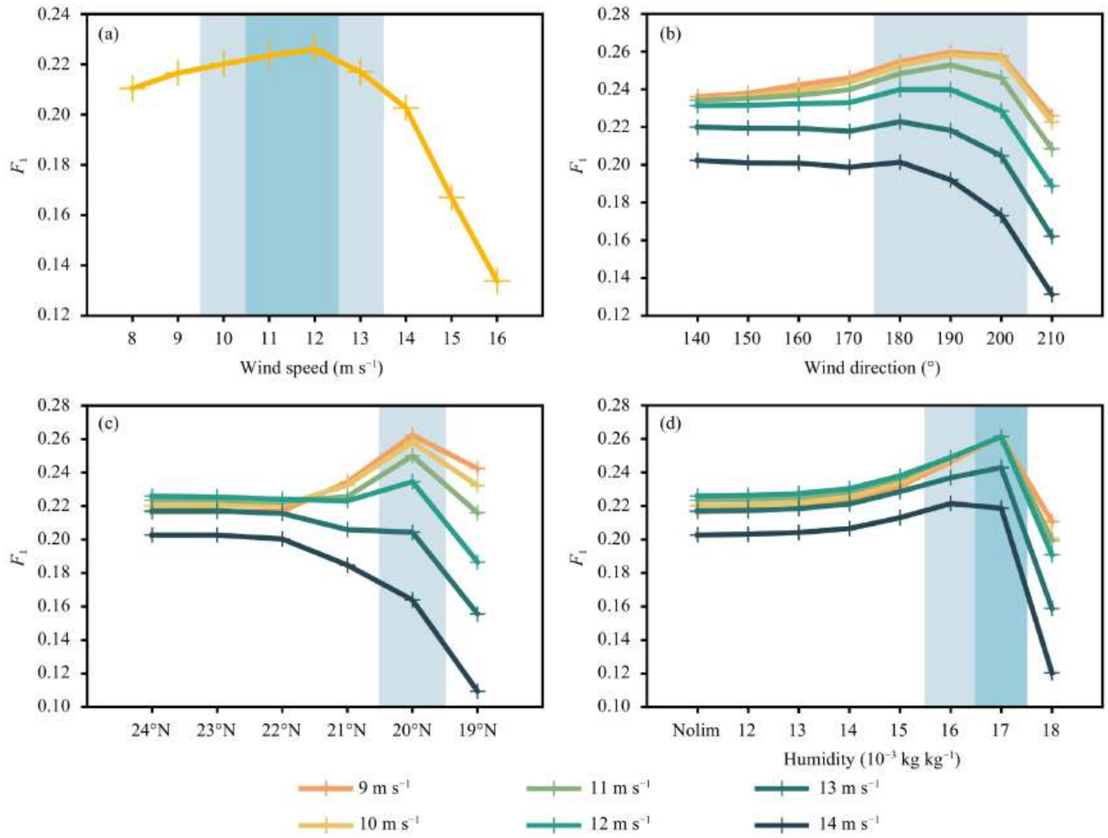

Fig. 11. Variability of F_1 score with threshold values of factors utilized to define the BLJ occurrence. These factors encompass the lower limits of (a) wind speed (m s^{-1}), (b) wind direction (°), (c) upper limit of latitude of jet core (°N), and (d) lower limit of humidity (10^{-3} kg kg^{-1}). The lines with different colors in (b–d) represent various wind speed thresholds for the BLJ.

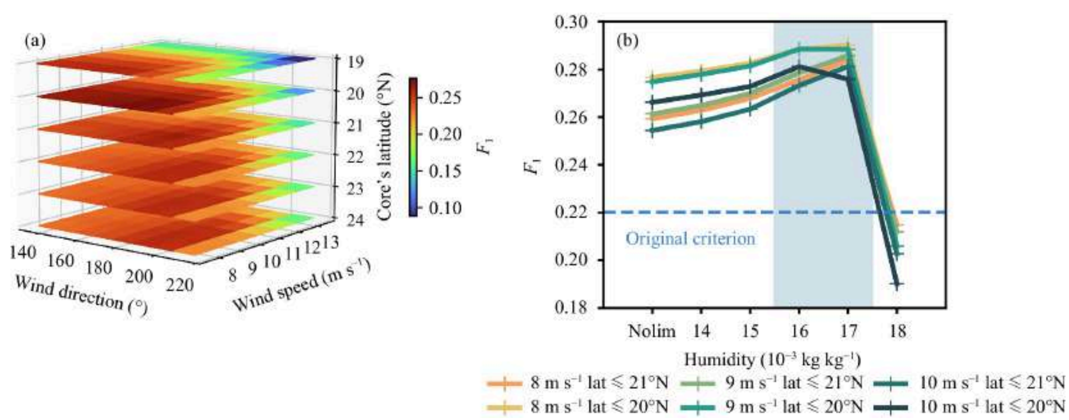

Fig. 12. (a) Variability of F_1 score with threshold values of wind speed (m s^{-1}) of BLJ, the BLJ wind direction (°), and upper limit of latitude of jet core (°N). These threshold values are used in conjunction to define the BLJ. (b) Variability of F_1 score after optimizing wind speed, wind direction (180°–270°), and maximum latitude thresholds and incorporating minimum humidity (10^{-3} kg kg^{-1}) thresholds.

ude of the jet core, and humidity thresholds. It shows that an optimal combination includes a wind speed threshold of 8–10 m s^{-1}, wind direction between 180° and 270°, and a jet core located below 21°N (for wind speed threshold of 10 m s^{-1}) or 20°N (for wind speed threshold of 8–9 m s^{-1}). When humidity is further considered (Fig. 12b), the F_1 score can be further improved with an optimal humidity threshold of 0.016–0.017 kg kg^{-1}. The final F_1 score after integrating multiple factors associated with BLJs can reach 0.29, representing nearly a 32% improvement over the initial score of 0.22. Therefore, this combination maximizes the F_1 score, enhancing the correlation between BLJs and HR events. However, it is important to note that despite the optimization of BLJ identification, the F_1 values remain relatively low in objective terms. This can be attributed to the unavoidable high false alarm rates, as the number of identified BLJ events significantly exceeds the number of HR events. This highlights the need for further refinement in future studies, particularly in understanding the mechanism of coastal precipitation.

6. Discussion and summary

This study utilizes 22-yr TRMM satellite rainfall data with a temporal resolution of 3 h and ERA5 reanalysis data to examine the intricate relationship between the boundary layer jets over the northern South China Sea and instances of heavy rainfall (HR) along the coast in Southern China (Yangjiang). A confusion matrix technique is employed to analyze the occurrence of HR based solely on the presence of BLJ. The relationship between BLJ and HR has led to the classification of four distinct scenarios: BLJ-HR, NoBLJ-HR, BLJ-NoHR, and NoBLJ-NoHR.

The mere presence of BLJ does not guarantee coastal HR; accurate HR prediction necessitates the consideration of other factors, particularly humidity. Some BLJs exhibit strong wind velocities but lack significant moisture content. Moreover, the association between BLJ intensity and coastal convergence is intricate. Strong BLJs can hinder coastal convergence due to their high intensity and northern core locations. This can cause them to cross the blockage of mountains near Yangjiang and even Nanling Mountain, affecting precipitation distribution to the north. Conversely, coastal HR can occur in the absence of BLJ if there are moderately weak southerly boundary-layer winds and a deep humidity background. This indicates the compensatory role of thermal forcing under suboptimal dynamic conditions.

Discrepancies in BLJ attributes between HR and non-HR events, such as intensity, wind direction, and spatial location, are found for sensitivity assessments aimed at enhancing the correlation between the two. The sensitivity assessments demonstrate varying relevance for different criteria associated with each BLJ attribute. The strongest correlation is achieved by simultaneously adjusting thresholds for BLJ intensity, wind direction, location, and humidity-related factors. The optimized thresholds incorporate a maximum wind speed threshold of 8–10 m s^{-1}, a wind direction spanning 180°–270°, and a jet core's maximum latitude of 21°N (for wind intensity threshold of 10 m s^{-1}) or 20°N (for wind intensity threshold of 8–9 m s^{-1}). Further refinement is achieved by introducing a moisture threshold of 0.017 or 0.016 kg kg^{-1} as part of the BLJ's criteria, leading to an additional measurable improvement in relevance to HR. While using BLJ as a singular factor for inferring HR occurrence is an ideal approach, a dramatic enhancement in prediction is not anticipated compared to numerical weather prediction or machine learning models. Nevertheless, this represents an initial step in gradually improving heavy rainfall prediction based on these known key factors.

Notably, the exploration of the relationship between BLJ and HR in this study hinges on BLJ identified from historical ERA5 reanalysis data. This study aims to establish a dependable framework for practical forecasting. A future practical scenario that actually delivers on these insights could be: (1) subjectively adjusting HR prediction based on the key indicator, BLJ, from numerical model forecasting; (2) estimating HR using artificial intelligence (AI)-based prediction data (like Pangu-Weather), encompassing wind fields and other meteorological fields, which might be straightforward and feasible for weather forecasters.

It is imperative to acknowledge that this approach exclusively focuses on inferring the occurrence of HR, without investigating its evolution and precise location. Additionally, the study refrains from an in-depth exploration of the causal relationship between BLJ and HR, recognizing the intricate non-linear processes involved in HR generation. These limitations underscore the need for further research to address these issues and further enhance the precision of the forecasting approach.

Acknowledgments. The authors acknowledge the high-performance computing support from School of Atmospheric Science of Sun Yat-sen University.

REFERENCES

Bao, M., 2007: The statistical analysis of the persistent heavy rain in the last 50 years over China and their backgrounds on the large scale circulation. *Chinese J. Atmos. Sci.*, **31**, 779–792, https://doi.org/10.3878/j.issn.1006-9895.2007.05.03.

Bi, K. F., L. X. Xie, H. H. Zhang, et al., 2023: Accurate medium-range global weather forecasting with 3D neural networks. *Nature*, **619**, 533–538, https://doi.org/10.1038/s41586-023-06185-3.

Blackadar, A. K., 1957: Boundary layer wind maxima and their significance for the growth of nocturnal inversions. *Bull. Amer. Meteor. Soc.*, **38**, 283–290, https://doi.org/10.1175/1520-0477-38.5.283.

Chakraborty, A., R. S. Nanjundiah, and J. Srinivasan, 2009: Impact of African orography and the Indian summer monsoon on the low-level Somali jet. *Int. J. Climatol.*, **29**, 983–992, https://doi.org/10.1002/joc.1720.

Chen, C. S., Y. L. Chen, C. L. Liu, et al., 2007: Statistics of heavy rainfall occurrences in Taiwan. *Wea. Forecasting*, **22**, 981–1002, https://doi.org/10.1175/WAF1033.1.

Chen, G. X., R. Y. Lan, W. X. Zeng, et al., 2018: Diurnal variations of rainfall in surface and satellite observations at the monsoon coast (South China). *J. Climate*, **31**, 1703–1724, https://doi.org/10.1175/JCLI-D-17-0373.1.

Chen, G. X., Y. Du, and Z. P. Wen., 2021: Seasonal, interannual, and interdecadal variations of the East Asian summer monsoon: A diurnal-cycle perspective. *J. Climate*, **34**, 4403–4421, https://doi.org/10.1175/JCLI-D-20-0882.1.

Dong, F., X. F. Zhi, L. Zhang, et al., 2021: Diurnal variations of coastal boundary layer jets over the northern South China Sea and their impacts on diurnal cycle of rainfall over southern China during the earlysummer rainy season. *Mon. Wea. Rev.*, **149**, 3341–3363, https://doi.org/10.1175/MWR-D-20-0292.1.

Du, Y., and G. X. Chen, 2018: Heavy rainfall associated with double low-level jets over southern China. Part I: Ensemble-based analysis. *Mon. Wea. Rev.*, **146**, 3827–3844, https://doi.org/10.1175/MWR-D-18-0101.1.

Du, Y., and G. X. Chen, 2019a: Heavy rainfall associated with double low-level jets over southern China. Part II: Convection initiation. *Mon. Wea. Rev.*, **147**, 543–565, https://doi.org/10.1175/MWR-D-18-0102.1.

Du, Y., and G. X. Chen, 2019b: Climatology of low-level jets and their impact on rainfall over southern China during the early-summer rainy season. *J. Climate*, **32**, 8813–8833, https://doi.org/10.1175/JCLI-D-19-0306.1.

Du, Y., and R. Rotunno, 2014: A simple analytical model of the nocturnal low-level jet over the Great Plains of the United States. *J. Atmos. Sci.*, **71**, 3674–3683, https://doi.org/10.1175/JAS-D-14-0060.1.

Du, Y., G. X. Chen, B. Han, et al., 2020a: Convection initiation and growth at the coast of South China. Part I: Effect of the marine boundary layer jet. *Mon. Wea. Rev.*, **148**, 3847–3869, https://doi.org/10.1175/MWR-D-20-0089.1.

Du, Y., G. X. Chen, B. Han, et al., 2020b: Convection initiation and growth at the coast of South China. Part II: Effects of the terrain, coastline, and cold pools. *Mon. Wea. Rev.*, **148**, 3871–3892, https://doi.org/10.1175/MWR-D-20-0090.1.

Du, Y., Y. L. Chen, and Q. H. Zhang, 2015: Numerical simulations of the boundary layer jet off the southeastern coast of China. *Mon. Wea. Rev.*, **143**, 1212–1231, https://doi.org/10.1175/MWR-D-14-00348.1.

Du, Y., Y. A. Shen, and G. X. Chen, 2022: Influence of coastal marine boundary layer jets on rainfall in South China. *Adv. Atmos. Sci.*, **39**, 782–801, https://doi.org/10.1007/s00376-021-1195-7.

Hastie, T., R. Tibshirani, and J. H. Friedman, 2009: *The Elements of Statistical Learning: Data Mining, Inference, and Prediction* (Vol. 2, pp. 1–758). New York, Springer, https://doi.org/10.1007/978-0-387-84858-7.

Holton, J. R., 1967: The diurnal boundary layer wind oscillation above sloping terrain. *Tellus*, **19**, 200–205, https://doi.org/10.1111/j.2153-3490.1967.tb01473.x.

Huang, X. G., C. Zhang, J. F. Fei, et al., 2022: Uplift mechanism of coastal Extremely Persistent Heavy Rainfall (EPHR): The key role of low-level jets and ageostrophic winds in the boundary layer. *Geophys. Res. Lett.*, **49**, e2021GL096029, https://doi.org/10.1029/2021GL096029.

Huffman, G. J., D. T. Bolvin, E. J. Nelkin, et al., 2007: The TRMM multisatellite precipitation analysis (TMPA): Quasi-global, multiyear, combined-sensor precipitation estimates at fine scales. *J. Hydrometeor.*, **8**, 38–55, https://doi.org/10.1175/JHM560.1.

Jiang, Q. F., S. P. Wang, and L. O'Neill, 2010: Some insights into the characteristics and dynamics of the Chilean low-level coastal jet. *Mon. Wea. Rev.*, **138**, 3185–3206, https://doi.org/10.1175/2010MWR3368.1.

Kalverla, P. C., J. B. Duncan Jr., G. J. Steeneveld, et al., 2019: Low-level jets over the North Sea based on ERA5 and observations: together they do better. *Wind Energy Science*, **4**, 193–209, https://doi.org/10.5194/wes-4-193-2019.

Kong, H., Q. H. Zhang, Y. Du, et al., 2020: Characteristics of coastal low-level jets over Beibu Gulf, China, during the early warm season. *J. Geophys. Res. Atmos.*, **125**, e2019JD031918, https://doi.org/10.1029/2019JD031918.

Li, J., and Y. L, Chen., 1998: Barrier jets during TAMEX. *Mon. Wea. Rev.*, **126**, 959–971, https://doi.org/10.1175/1520-0493(1998)126<0959:BJDT>2.0.CO;2.

Li, X. Q., and Y. Du, 2021: Statistical relationships between two types of heavy rainfall and low-level jets in South China. *J. Climate*, **34**, 8549–8566, https://doi.org/10.1175/JCLI-D-21-0121.1.

Liu, X., Y. L. Luo, L. Huang, et al., 2020: Roles of double low-level jets in the generation of coexisting inland and coastal heavy rainfall over south China during the presummer rainy season. *J. Geophys. Res. Atmos.*, **125**, https://doi.org/10.1029/2020JD032890.

Murphy, K. P., 2012: *Machine Learning: A Probabilistic Perspective*. MIT Press, 1104 pp.

Powers, D. M. W., 2011: Evaluation: from precision, recall and F-measure to ROC, informedness, markedness and correlation. ArXiv, abs/2010.16061, https://doi.org/10.48550/arXiv.2010.16061.

Shapiro, A., E. Fedorovich, and S. Rahimi, 2016: A unified theory for the Great Plains nocturnal low-level jet. *J. Atmos. Sci.*, **73**, 3037–3057, https://doi.org/10.1175/JAS-D-15-0307.1.

Shen, Y., A. Y. Xiong, Y. Wang, et al., 2010: Performance of high-resolution satellite precipitation products over China. *J. Geophys. Res. Atmos.*, **115**, D02114, https://doi.org/10.1029/2009JD012097.

Shen, Y. A., and Y. Du, 2023: Sensitivity of boundary layer parameterization schemes in a marine boundary layer jet and associated precipitation during a coastal warm-sector heavy rainfall event. *Front. Earth Sci.*, **10**, 1085136, https://doi.org/10.3389/feart.2022.1085136.

Sokolova, M., and G. Lapalme, 2009: A systematic analysis of performance measures for classification tasks. *Information processing & management*, **45**, 427–437, https://doi.org/10.1016/j.ipm.2009.03.002.

Tao, S.-Y., 1980: *Rainstorms in China*. Science Press, 225 pp. (in Chinese)

Townsend, J. T., 1971: Theoretical analysis of an alphabetic confusion matrix. *Perception & Psychophysics*, **9**, 40–50, https://doi.org/10.3758/bf03213026.

Zhang, L., X. Y. Ma, S. P. Zhu, et al., 2022: Analyses and applications of the precursor signals of a kind of warm sector heavy rainfall over the coast of Guangdong, China. *Atmos. Res.*, **280**, 106425, https://doi.org/10.1016/j.atmosres.2022.106425.

Zhang, X., Y. Luo, and Y. Du, 2024: Observation of boundary-layer jets in the northern South China Sea by a research vessel. *Remote Sensing*, **16**, 3872, https://doi.org/10.3390/rs16203872.

Journal of Meteorological Research

Vol. 39 No. 1 February 2025

CONTENTS

CELEBRATING 100 YEARS OF THE CHINESE METEOROLOGICAL SOCIETY'S JOURNAL—*ACTA METEOROLOGICA SINICA*

ORIGINAL PAPER

Chief Editor: Zhemin TAN Published Since 1987
Superintended by China Association for Science and Technology
Sponsored by Chinese Meteorological Society
Edited and Published by Editorial Office of *Journal of Meteorological Research*
Co-Published by Springer Nature
Produced by Beijing Renhe Information Technology Co. Ltd.
Printed by Beijing BOHS Color Printing Co. Ltd.
Domestically Distributed by China Science Publishing & Media Ltd.
Internationally Distributed by Springer Nature
Online Submission: http://jmr.cmsjournal.net
Domestic Register Number: CN 11-2277/P
Publication Date: 24 February 2025 (Vol. 39, No. 1)
Domestic Subscription Price: 450 RMB per year (bimonthly published, 6 issues)

WeChat

Domestic Purchase

Cover designed by Yuxiang ZHU

Journal of Meteorological Research

http://jmr.cmsjournal.net

http://link.springer.com/journal/13351

ISSN 2095-6037

02>

9 772095 603251

JMR Journal of Meteorological Research

The Relationship Scenarios between Boundary Layer Jet and Coastal Heavy Rainfall during the Pre-Summer Rainy Season of South China

Yu DU, Siyang YI

Citation: Du, Y. and S. Y. Yi, 2025: The relationship scenarios between boundary layer jet and coastal heavy rainfall during the pre–summer rainy season of South China. *J. Meteor. Res.*, **39**(1), 26–40, doi: 10.1007/s13351-025-4138-x

View online: http://jmr.cmsjournal.net/article/doi/10.1007/s13351-025-4138-x